ACS OMEGA

Article

Cite This: ACS Omega 2019, 4, 19106−19115

http://pubs.acs.org/journal/acsodf

Nitrone-Modified Gold Nanoparticles: Synthesis, Characterization, and Their Potential as ^{18}F-Labeled Positron Emission Tomography Probes via I-SPANC

Sara Ghiassian,[†] Lihai Yu,[‡] Pierangelo Gobbo,[†,∥] Ali Nazemi,[†,⊥] Tommaso Romagnoli,[†] Wilson Luo,[†] Leonard G. Luyt,*[,†,‡,§] and Mark S. Workentin*[,†]

[†]Department of Chemistry and the Center for Materials and Biomaterials Research and [§]Department of Oncology, The University of Western Ontario, London N6A 5B7, Ontario, Canada

[‡]London Regional Cancer Program, 800 Commissioners Rd. E., London N6A 5W9, Ontario, Canada

Supporting Information

ABSTRACT: A novel bioorthogonal gold nanoparticle (AuNP) template displaying interfacial nitrone functional groups for bioorthogonal interfacial strain-promoted alkyne−nitrone cycloaddition reactions has been synthesized. These nitrone−AuNPs were characterized in detail using ^{1}H nuclear magnetic resonance spectroscopy, transmission electron microscopy, thermogravimetric analysis, and X-ray photoelectron spectroscopy, and a nanoparticle raw formula was calculated. The ability to control the conjugation of molecules of interest at the molecular level onto the nitrone−AuNP template allowed us to create a novel methodology for the synthesis of AuNP-based radiolabeled probes.

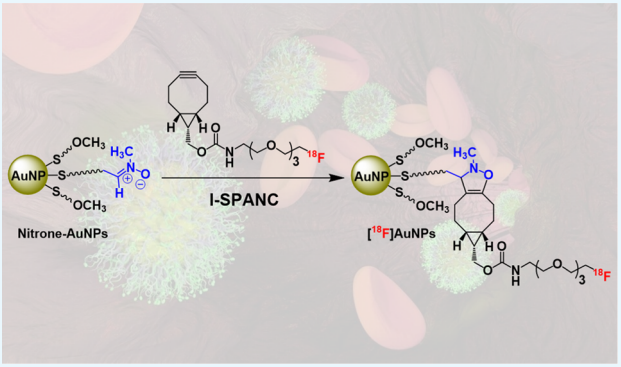

INTRODUCTION

Positron emission tomography (PET) is a noninvasive imaging technique that provides valuable real-time information on physiological, biochemical, and pharmacological processes that take place in living organisms.[1−6] The engineering and synthesis of radiolabeled probes for medical imaging with PET is an area of chemistry that is extremely active and rich in challenges, which includes solubility and biological stability, control of biodistribution, and preserving molar activity. Among the different PET radionucleotides, the most employed is fluorine-18 (^{18}F) because of its particularly favorable nuclear and chemical properties: it offers a half-life of 110 min, a β^{+}-branch of 97%, and a low β^{+}-energy of 635 keV. This allows for its facile off-site production and transportation, for relatively long imaging experiments, and the acquisition of images with higher resolution than those obtained using other radionuclides.[7]

One of the most common strategies for the synthesis of robust and efficient PET probes involves the use of radiolabeled prosthetic groups that are then introduced onto the biomolecular system of interest in the last step of synthesis. This type of synthesis involves a continuous race against time and the decay of the radionuclide. In fact, the biggest challenge involves the development of synthetic steps with high reaction rates, high yields, and that take place under mild reaction conditions while using sub-micromolar amounts of radiolabeled compounds.[7−18]

In recent years, bioorthogonal chemistry has started to revolutionize the synthesis of radiolabeled probes, in particular for higher molecular weight biologics. In fact, bioorthogonal reactions represent ideal candidates for those critical synthetic steps because of their robustness, versatility, fast kinetics, high yields, and mild conditions. Most importantly, they have the potential to lead to easier and faster synthetic protocols for the synthesis of radioactive biologics and nanoparticles, with straightforward and approachable methods for users with basic chemistry skills.

One of the most useful bioorthogonal reactions is the strain-promoted alkyne−azide cycloaddition (SPAAC). This is a variation of the copper (I)-catalyzed Huisgen cycloaddition (CuAAC), whose driving force relies on a strained C−C triple bond imbedded in an eight-membered ring. Most importantly, the SPAAC reaction does not require the use of cytotoxic metal catalysts, overcoming the problems associated with their application, such as cytotoxicity, copper-promoted degradation of peptides and proteins, and formation of insoluble copper acetylide.[19−22] The typical complementary functional group or chemical reporter of the strained alkyne is the azide because of its small dimension, stability, and biological inertness. However, utilizing more reactive alternatives to azides can greatly enhance the reaction rate of strain-promoted cyclo-

Received: July 24, 2019
Accepted: October 28, 2019
Published: November 8, 2019

DOI: 10.1021/acsomega.9b02322
ACS Omega 2019, 4, 19106−19115

Scheme 1. Synthesis of Nitrone−AuNPs; Top: Synthetic Strategy for the Preparation of the Nitrone-Terminated Thiol Ligand 4[a]

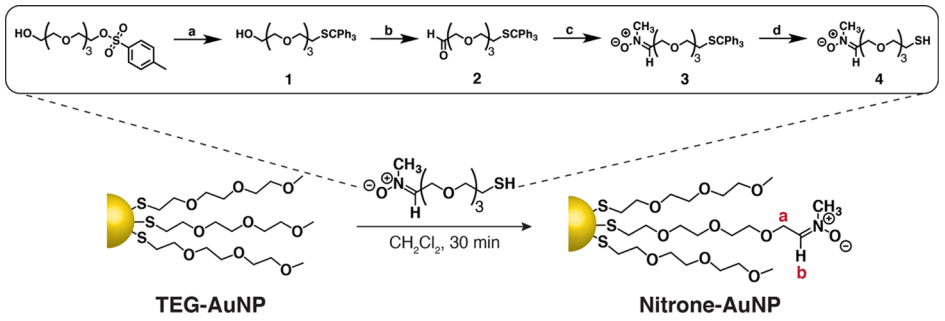

[a]Reaction conditions: (a) Ph_3CSH, NaOH, EtOH/benzene; (b) P_2O_5, DMSO, Et_3N, CH_2Cl_2; (c) CH_3NHOH, Et_3N, CH_3CN; (d) TFA/CH_2Cl_2, iPr_3SiH.

addition, with the potential of impacting even more the synthesis of radiolabeled probes.

Recently, a variant to SPAAC has been proposed, which replaces the azido functionality with a stable and biocompatible nitrone group. The bioorthogonal strain-promoted alkyne−nitrone cycloaddition (SPANC) reaction represents an improvement of the SPAAC because of its faster reaction kinetics as well as tunability of the nitrone moiety by using diverse substituents on both carbon and nitrogen atoms of the dipole.[23,24] The SPANC reaction has quickly found applications that range from protein modification[25,26] and cell surface labeling,[24] to materials science[27] and radiolabelling.[9−18,28] Nevertheless, it is surprising how to date it has not found an application in the synthesis of radiolabeled nanomaterials.

With the final goal of engineering radiolabeled contrast agents with higher spatial and temporal resolution, in recent years, radiochemists have started to approach the field of nanomaterials because of their attractive physical, chemical, and biological properties.[29−31] In particular, gold-based nanomaterials represent an ideal multitasking imaging probe because of their stability, biocompatibility, facile conjugation to biomolecules, and their unique physical−chemical properties. These characteristics make them useful as multimodal contrast agents and as photodynamic therapy-contrast agents.[32−37] An additional characteristic that makes them desirable in the field of biomedical imaging is that their size, shape, and surface charge can be easily tuned through the synthesis, and the cellular and tissue uptake can potentially be regulated.[35,38−41]

Normally, gold nanomaterials-based radiolabeled probes are synthesized either by deposition of a radioactive element (e.g., ^{64}Cu, ^{125}I, and ^{198}Au) onto the nanostructure[35,36,38,42,43] or by conjugating chelating agents (e.g., DOTA) or prosthetic groups carrying the radioactive element onto the nanomaterial corona.[39,44] However, the former methodology has the drawback that the size and shape of the nanomaterial substrate can change during the redox reaction, causing destabilization of the nanoparticle or irreversible aggregation.[38] As a consequence, the precise characterization of both the metallic core and organic corona becomes extremely challenging or even impossible. The latter method instead relies on a "shotgun-type" conjugation approach, which has no control over the extent of incorporation of the desired radiolabeled prosthetic group or its quantification, representing a major issue for potential therapeutic applications.[39,44,45]

In the past few years, the Workentin research group has begun to develop a toolbox of bioorthogonal nanomaterial templates. These are stable (i.e., can be stored for indefinitely long periods of time under appropriate conditions) and biocompatible nanomaterials that display interfacial bioorthogonal moieties that are ready to react with any molecular system of interest that carries the complementary functional group or chemical reporter. The bioorthogonal nanomaterial template allows for the facile and covalent modification of the nanomaterial's surface with reactions that are chemoselective, biocompatible, fast, high yielding, and, most importantly, orthogonal to the surface chemistry of the nanomaterial.[46−52]

In this study, we further expanded the members of this bioorthogonal nanomaterial toolbox and synthesized and characterized small (∼3 nm) AuNPs functionalized with interfacial nitrone functional groups (nitrone−AuNPs) for interfacial SPANC (I-SPANC) reactions. This new bioorthogonal AuNP template is extremely resilient because the gold core is protected by a monolayer of tri- and tetra-ethylene glycol-based thiolated ligands (see Scheme 1). This allows the nitrone−AuNPs to be stored indefinitely at −20 °C and be repeatedly dried and redissolved in polar organic solvents and water with little to no aggregation. The nitrone−AuNPs could be completely characterized, thanks to the discrete size of their thiolated ligands, and the number of interfacial nitrone moieties could be determined with good precision, including the determination of a nanoparticle's raw formula. This allowed us to investigate in detail the interfacial reactivity of the nitrone−AuNP template toward the I-SPANC reaction using model molecules. Subsequently, we determine a facile protocol for the realization of ^{18}F-decorated AuNPs ([^{18}F]-AuNPs) based on an I-SPANC reaction between the bioorthogonal nitrone−AuNP template and a radiolabeled prosthetic group carrying a bicyclononyne (BCN) moiety. The [^{18}F]AuNPs showed a wide biodistribution profile upon in vivo experiments. This is most likely because of the small dimension of the nanomaterial and the ethylene glycol-based coating, which increases the nanomaterial biocompatibility, hinders protein absorption, and increases blood circulation time.[53] Our approach to modification of nanomaterial interfaces ensures molecular level control over the functionalization of the AuNPs with the ^{18}F-functionalized-BCN prosthetic group and overcomes the drawbacks of the current synthetic methodologies present in the literature. Lastly, the ability of our ^{18}F-functionalized-BCN to react broadly with azides and nitrones opens exciting opportunities for the modification of other biologically relevant materials because of the ease with which azido and nitrone moieties can be synthetically incorporated.

DOI: 10.1021/acsomega.9b02322
ACS Omega 2019, 4, 19106−19115

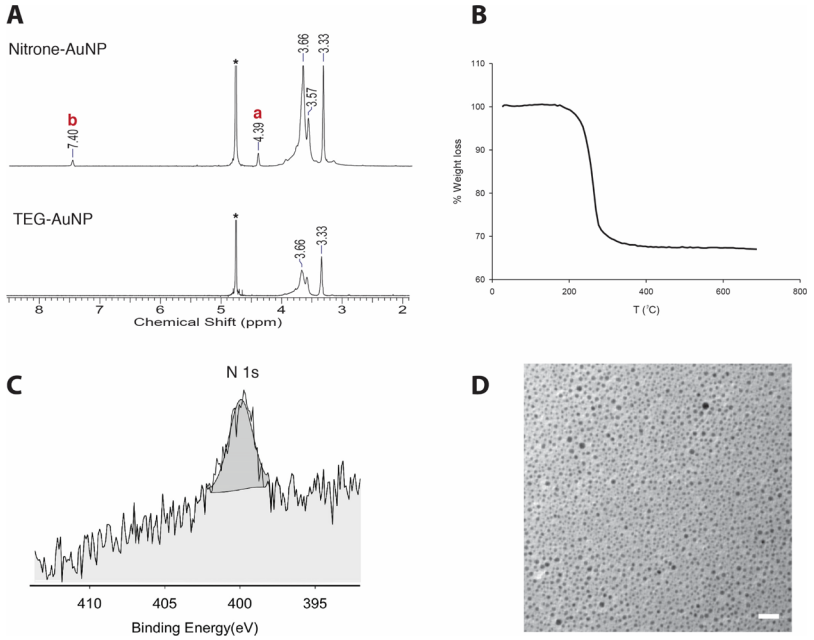

Figure 1. Characterization of nitrone−AuNPs. (A) ^{1}H NMR spectra recorded in D_2O and referenced against residual water (*) of nitrone−AuNP (top) and TEG−AuNP starting material (bottom). The peaks corresponding to the protons of the nitrone moiety are labeled with alphabetical letters and correspond to the protons highlighted in Scheme 1. (B) TGA of nitrone-AuNPs recorded under a stream of nitrogen gas. (C) nitrone−AuNP's high-resolution XPS scan of the N 1s peak. (D) Typical TEM image of nitrone−AuNPs (scale bar 20 nm).

Thus, the methodology reported herein represents a general protocol for the preparation of more structurally diverse and functional ^{18}F-labeled PET probes.

RESULTS AND DISCUSSION

The method for the introduction of the nitrone moiety onto the AuNP's surface requires the synthesis of the appropriate thiol-containing ligand to be used for the ligand exchange reaction with a 3 nm triethylene glycol monomethyl ether AuNP (TEG−AuNP) starting material. The TEG−AuNPs represent an ideal substrate for the synthesis of a bioorthogonal nanomaterial template because of their approachable synthesis, the possibility to synthesize them in the gram scale, and the possibility of using spectroscopic techniques [e.g., nuclear magnetic resonance (NMR) spectroscopy, Fourier transform infrared (FT-IR) spectroscopy, X-ray photoelectron spectroscopy (XPS)] for characterizing them and following their interfacial reactivity. The TEG−AuNP template is amphiphilic and extremely resilient. In fact, TEG−AuNPs can be repeatedly dried and redissolved in water and different polar organic solvents, dissolved in strongly acidic[49] or basic solution,[54] heated at more than 100 °C for prolonged periods of time[55] with little to no aggregation, and be exposed to glutathione-rich aqueous environments with minimal evidence of ligand exchange as per ^{1}H NMR and fluorescence spectroscopy.[54] The ethylene glycol framework has also the potential function of prolonging the AuNP's circulation half-life, and reducing the AuNP's immunogenicity, making the nanosystem suitable for many applications in both chemical biology and nanomedicine.[56−58] The desired nitrone-terminated ligand **4** was designed with a tetraethylene glycol unit that separates the thiol head from the nitrone moiety (see Scheme 1). The ethylene glycol linker preserves the physical−chemical and biological properties of the AuNPs, ensures good packing of the monolayer around the gold core, and, because of the extra ethylene glycol unit, it allows the nitrone group to extend out of the corona and be more accessible to react through the I-SPANC. It is worth noting that the complementary system in which AuNPs are functionalized with strained alkynes capable of reacting with [^{18}F]-bearing nitrones is also possible. However, this presents additional synthetic challenges relating to undesired side reactivity of the strained C−C triple bond toward the nucleophilic −SH. More importantly, we wished to preserve the generality of the [^{18}F]-bearing prosthetic group, which can react broadly with azides and nitrones. Because of the chemical stability and ease-of-introduction of azide and nitrone groups onto diverse materials, we envisioned this represents a more general protocol for the preparation of functional PET probes.

The synthetic strategy for the synthesis of the nitrone-terminated thiol ligand **4** is reported in Scheme 1. Briefly, tetraethylene glycol-monosulfonate HO−EG_4−OTos was treated with triphenylmethanethiol to prepare the protected thiol HO−EG_4−$SCPh_3$ **1**. The alcohol moiety of compound **1** was then oxidized to aldehyde using dimethyl sulfoxide (DMSO) and phosphorus pentaoxide. Aldehyde **2** was reacted with *N*-methyl hydroxylamine hydrochloride in the presence of a base to afford nitrone **3**. Finally, the desired nitrone-terminated thiol ligand **4** was synthesized by deprotecting nitrone **3** in CH_2Cl_2/5% trifluoroacetic acid (TFA). Details of the synthetic procedure can be found in the Supporting Information. Subsequently, a ligand exchange reaction was used to incorporate the nitrone-terminated thiol **4** onto the TEG−AuNPs (see Scheme 1). The ligand exchange reaction was carried out by stirring a solution of TEG−AuNPs and ligand **4** (1:6 AuNPs to ligand **4** ratio) in CH_2Cl_2 for 30 min. After removing the solvent, the resulting film of AuNPs was washed with a mixture of 10:1 hexanes/isopropanol five times in order to remove any free thiol or disulfide. Finally, the nitrone−AuNPs were further purified by dialysis in Milli-Q water overnight. The resulting nitrone−AuNPs retained the

DOI: 10.1021/acsomega.9b02322
ACS Omega 2019, 4, 19106−19115

Scheme 2. Synthesis of [^{19}F]AuNPs; Top: Synthetic Strategy for the Preparation of the ^{19}F-Containing Prosthetic Group Compound [^{19}F]13[a]

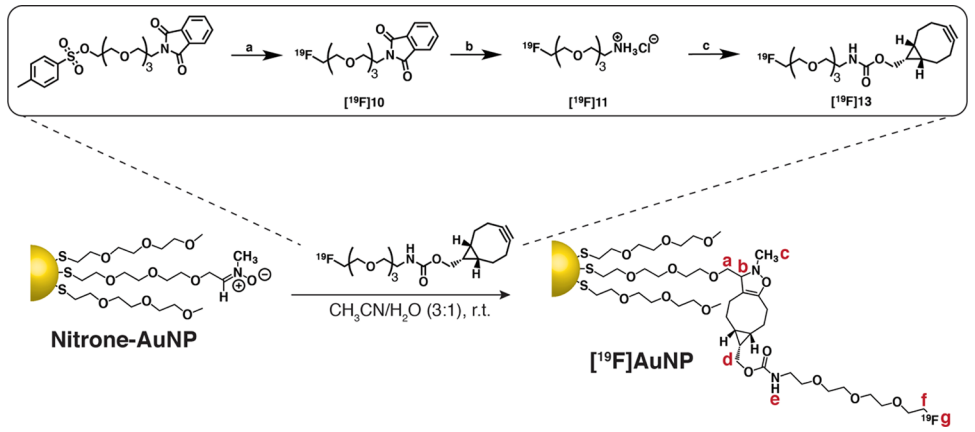

[a]Reaction conditions: (a) CsF, *t*BuOH, 60 °C, 5 h; (b) $H_2N-NH_2\cdot H_2O$, 95% EtOH, reflux, 5 h; (c) compound **12**, Et_3N, DMF, 0 °C, 20 min. Bottom: characterization of [^{19}F]AuNPs.

solubility properties of the TEG−AuNP starting material, being soluble in water and polar organic solvents.

Characterization of the nitrone−AuNPs was achieved using ^{1}H NMR spectroscopy, transmission electron microscopy (TEM), thermogravimetric analysis (TGA), and XPS. Initially, the success of the place exchange reaction was confirmed using ^{1}H NMR spectroscopy, see Figure 1. The ^{1}H NMR spectrum of the nitrone−AuNPs recorded in D_2O exhibited the expected broad peaks at δ_H: 3.3−3.8 ppm because of the protons of the ethylene glycol units. Additionally, new signals appeared after the exchange reaction at δ_H: 7.4 and 4.4 ppm in a 1:2 ratio and corresponded to the proton α to the nitrogen (H_b) and the two protons of the methylene group next to the nitrone functionality (H_a), respectively, confirming the presence of the nitrone moiety on the AuNPs' corona. The lack of sharp signals in the ^{1}H NMR spectrum of the nitrone−AuNPs indicates that there was no free thiol present and confirmed the efficiency of our cleaning protocol. Furthermore, the nitrone−AuNP sample was monitored over an extend period of time by ^{1}H NMR spectroscopy and there was no evidence of free thiols, indicating very good stability of the nanoparticle's corona. Additionally, we observed no hydrolysis of the interfacial nitrone moiety as indicated by no disappearance of the nitrone's Cα−H signal or appearance of an aldehyde proton signal. Through the integration of the signal at δ_H: 7.4 ppm, correlating to H_b, and the integration of the signal at 3.3 ppm, corresponding to the three protons of the terminal methyl group of the base MeO−EG_3−S^- ligands, it was determined that the 18 ± 2% of the thiolated ligands that compose the nanoparticle's organic corona comprised nitrone-terminated ligand **4**, whereas 82 ± 2% consisted of the base MeO−EG_3−S^- ligand.

Further information about the quantity and ratio of the thiolated ligands that compose the organic corona could be obtained from the thermogravimetric curve. The TGA showed that 33% of the mass of a nitrone−AuNP is composed by the organic corona, see Figure 1. The first derivative of the thermogravimetric curve (see Figure S2) showed two distinct components that were related to the two thiolated ligands: the nitrone-terminated ligand **4** and the base MeO−EG_3−S^- ligands.[48] By knowing the molecular weight of the two ligands, it was possible to calculate that 20% of the total number of ligands were nitrone−EG_4−S^- and 80% were MeO−EG_3−S^- ligands by mass. This was consistent with the analysis of the ^{1}H NMR spectrum of the nitrone−AuNP.

XPS analysis further confirmed the successful preparation of nitrone−AuNPs and the ratio between the two different thiolated ligands (see Figures 1 and S3). The Au 4f region exhibited a pair of peaks at 84.3 and 87.6 eV assigned to the Au $4f_{7/2}$ and Au $4f_{5/2}$ peaks, respectively, which were originated by the AuNP cores and were shifted at higher binding energy (BE) because of the nanoparticle size effect.[59] The S 2p core line showed the presence of two components, the S $2p_{3/2}$ at 162.8 eV and S $2p_{1/2}$ at 164.0 eV, in a 2:1 spin orbit splitting ratio related to the Au−S bonds.[60] The absence of additional components in the region 163−165 and 168−170 eV confirmed that there are no free thiols and that our cleaning procedure was effective. Additionally, the XPS survey spectrum of nitrone−AuNPs clearly showed the appearance of a nitrogen peak at 399.9 eV (N 1s) with 0.6 at. %, confirming the incorporation of the nitrone group. Furthermore, from the sulphur to nitrogen ratio it was possible to calculate that 20% of the total ligands on the gold core consisted of nitrone−EG_4−SH, and this information was in line with the results obtained independently through ^{1}H NMR spectroscopy and TGA.

Finally, TEM images of nitrone−AuNPs showed that their gold core is 2.6 ± 0.5 nm wide (Figure 1). By combining the information obtained through ^{1}H NMR spectroscopy, TEM imaging, and TGA, and assuming that the AuNPs have a spherical shape and are perfectly monodispersed in size, it was possible to calculate a raw formula for the nitrone−AuNPs of Au_{500}(MeO−EG_3−S^-)$_{200}$(nitrone−EG_4−S^-)$_{40}$.[61] Details of the calculations can be found in the Supporting Information.

It is worth noting that the amount of nitrone moieties at the AuNP's interface can be easily tuned through the ligand exchange by changing the reaction time and the gold to ligand **4** ratio (see Figure S1). However, it was found that as we increased the concentration of nitrone ligand **4** in excess of 30% (by mole relative to MeO−EG_3−S^- in the monolayer), the resulting AuNPs were exclusively soluble in water. Although this increased hydrophilicity would be desirable for in vivo applications, because of hydrophobicity of the [^{18}F]-BCN prosthetic group, the resulting isoxazoline—formed by

DOI: 10.1021/acsomega.9b02322
ACS Omega 2019, 4, 19106−19115

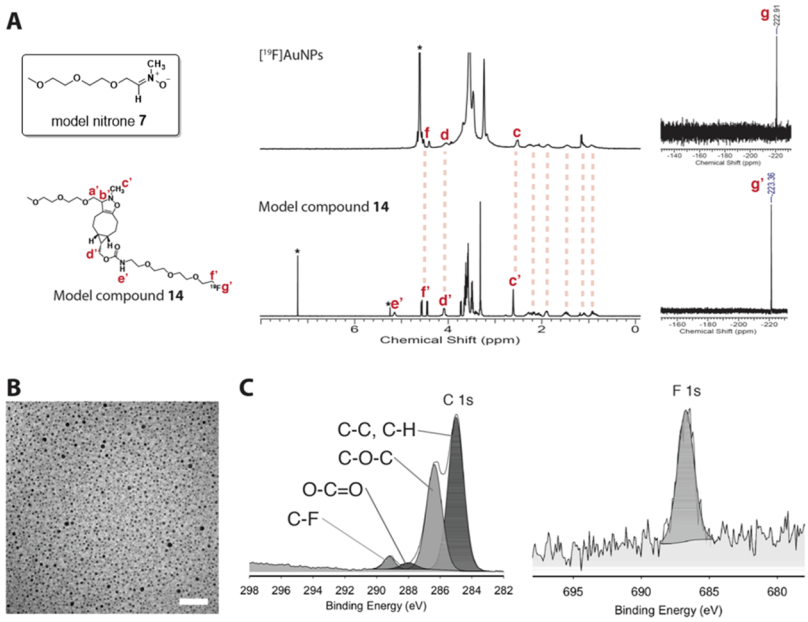

Figure 2. Characterization of [^{19}F]AuNPs. (A) ^{1}H and ^{19}F NMR spectra recorded in D_2O and $CDCl_3$ for [^{19}F]AuNPs (top) and model compound **14** (bottom) and referenced against residual solvents (*); (B) typical TEM image of [^{19}F]AuNPs (scale bar 20 nm); (C) high-resolution XPS scan of C 1s and F 1s peaks for [^{19}F]AuNPs.

interfacial SPANC—may display weaker water solubility. Therefore, it is of paramount importance that the nitrone–AuNPs retain their amphiphilicity in order to be used as phase-transfer agents, and covalently bind those prosthetic groups in organic solvent and carry them in water media where they can be used for their designed application.

After confirming successful incorporation of nitrone moieties, we sought to evaluate the reactivity of nitrone–AuNPs toward interfacial SPANC (I-SPANC). Because of the clean and quantitative reactivity of SPANC,[23,24] the stoichiometric information of nitrone–AuNPs can be extended to establish the concentration of interfacial [^{18}F]. In order to do this and before undertaking any radiolabeled-AuNP in vivo experiments, we performed a proof of concept study using the fluorinated (^{19}F) strained alkyne **13** (Scheme 2). Compound **13** was designed with a tetraethylene glycol linker in between the strained alkyne moiety (a BCN) and the fluorine atom in order to increase its water solubility. The detailed synthesis and characterization of compound **13** is reported in the Supporting Information. Despite the high reactivity of BCN, compound **13** is stable for months and can be stored indefinitely at −20 °C.

Because we quantified with very good precision the amount of nitrone moieties per AuNP (0.840 μmol mg^{-1}), for our reactivity test, we were able to employ a 1:1 equivalent of strained alkyne **13** to interfacial nitrones. This is remarkable because it gives us unprecedented molecular level control over the synthesis of conjugated and labeled AuNPs, which will assist in the future generation of targeted agents while still controlling available nitrone sites for late-stage radiochemistry. For future investigations, this approach would also allow for the facile introduction of multiple molecular systems of interest simply by altering the molar ratio of complementary substrates. In a typical conjugation experiment, we mixed 10 mg of nitrone–AuNPs (8.4 μmol of nitrone) with 8.4 μmol of compound **13** in a mixture CH_3CN/H_2O 3:1 and at room temperature. Despite bearing the ethylene glycol linker in between the fluorine atom and the BCN moiety, compound **13** still required an organic solvent to be dissolved. In order to facilitate the characterization of the interfacial cycloaddition product and obtain proof of proper interfacial reactivity, we set up in parallel a control reaction using the model compound nitrone **7**. The ^{1}H NMR spectrum of the control reaction showed complete conversion to the cycloaddition product as demonstrated by the disappearance of the peaks of the starting materials, and the appearance of the NH peak at 5.2 ppm (H_e), of a doublet of triplets at 4.6 ppm belonging to CH_2 alpha to the [^{19}F] (H_f), of the BCN's CH_2 alpha to the carbamate moiety at 4.2 ppm (H_d), of isoxazoline's H_c at 2.7 ppm, and of BCN's multiplets in the 0.5–2.5 ppm region. The product of the control SPANC reaction was characterized also by ^{19}F NMR spectroscopy, which shows a fluorine peak at −223.4 ppm, and by ^{13}C NMR spectroscopy and mass spectrometry. All the analyses confirmed a successful SPANC reaction that proceeded cleanly and quantitatively with no generation of byproducts. Proof for a successful I-SPANC reaction at the AuNP's interface could then be obtained by comparing the ^{1}H NMR spectrum of the control reaction product with that of the [^{19}F]AuNPs. Figure 2 shows excellent correspondence between the typical broad peaks of the AuNP sample with those of the cycloaddition product **14**. Furthermore, the complete disappearance of the nitrone protons H_a and H_b confirms a quantitative and clean I-SPANC reaction. Complete labeling of the interfacial nitrone moieties with model compound strained alkyne **13** was observed within 20 min. This is consistent with our kinetics studies,[51] which showed a second-order rate constant in the range of 5×10^{-2} M^{-1} s^{-1}, and literature values.[62] It is worth noting that the ^{1}H NMR of the control reaction had to be recorded in $CDCl_3$ because of the limited water-solubility of compound **14**, whereas the ^{1}H NMR of the [^{19}F]AuNPs could be easily recorded in D_2O, highlighting the role of the nanocarrier as a phase-transfer agent.

DOI: 10.1021/acsomega.9b02322
ACS Omega 2019, 4, 19106−19115

Scheme 3. Synthesis of [^{18}F]AuNPs[a]

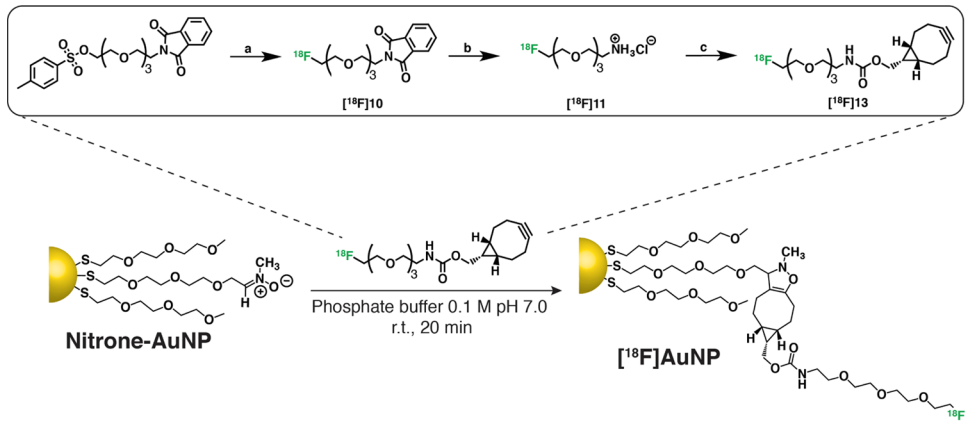

[a]Reaction conditions: (a) $^{18}F^-$, K_2CO_3, Krypofix222, CH_3CN, 90 °C, 5 min; (b) hydrazine, CH_3CN/36% H_2O/0.1% TFA, 60 °C, 5 min; (c) Compound **12**, Et_3N, CH_3CN, room temperature, 20 min; followed by 60 °C, 5 min

After the I-SPANC reaction was completed and before further characterization, in order to ensure complete removal of any residual free prosthetic group **13**, the [^{19}F]AuNPs were purified by washing the nanoparticles with a 10:1 hexanes/isopropanol mixture and by dialysis in water overnight. The purified [^{19}F]AuNPs were then characterized by XPS and TEM. The XPS data furnished additional proof of successful I-SPANC reaction (see Figure 2). The XPS survey of [^{19}F]AuNPs shows the appearance of a peak related to the fluorine at 686.7 eV, and the high-resolution scan of the C 1s peak exhibits the appearance of a component at 288.0 and 289.2 eV related to O−C*═O (carbamate group) and *C−F, respectively. The presence of the carbamate group is also confirmed by the appearance of a shoulder at 533.6 eV in the high-resolution scan of the O 1s peak. It should be noted that a new component for the C−N bond of the carbamate group should have appeared in the high-resolution scan of C 1s; however, such a component was not observed because it falls at the same BE region of the C−OH/O−C−O groups. Nonetheless, the presence of such a group is clearly shown in the high-resolution N 1s scan with a BE of ∼400 eV. Finally, TEM images (see Figure 2) show no change in size, shape, or size distribution for the [^{19}F]AuNPs compared to the nitrone−AuNPs starting material. This is because of the mild reaction condition required by the I-SPANC reaction. Together, these results confirmed unequivocally that the nitrone−AuNPs were able to react with the fluorinated compound **13** through the I-SPANC to give the corresponding cycloaddition product rapidly, cleanly, and quantitatively. Because the nitrone−AuNPs reacted quantitatively, we established that each AuNP is now carrying on average 40 [^{19}F] prosthetic groups, or ∼0.84 μmol of compound **13** per milligram of AuNPs. This information is of great importance for the use of the final [^{18}F]AuNP as a PET contrast agent and the development of targeted agents. Most importantly, no loss of thiolated ligands was observed by ^{1}H NMR spectroscopy (which would show appearance of sharp signals) over a period of 3 days at room temperature, indicating good stability of the nanomaterial and potential for in vivo studies.

Once we confirmed our ability to modify and quantify AuNPs with ^{19}F as a model via I-SPANC, we proceeded with the synthesis of the [^{18}F] analogue of prosthetic group **13**, its conjugation onto the nitrone−AuNPs, and the in vivo biodistribution investigation through PET imaging. The synthesis of [^{18}F]AuNPs is reported in Scheme 3, and it is based on the synthetic strategy for compound **13** with minor changes in order to satisfy the radiolabeling working conditions. Most importantly, from the step that introduces the fluorine atom on compound **9**, all the subsequent reactions leading to the [^{18}F]AuNPs PET agent rely on excellent reaction yields and very fast reaction kinetics to minimize decay of ^{18}F prior to injection. Finally, the [^{18}F]AuNPs were purified by size exclusion chromatography in order to remove any unreacted prosthetic group. The entire synthesis of the [^{18}F]AuNPs, from ^{18}F delivery until end-of-synthesis, was completed in 4 h and with specific activity of 52 MBq mg^{-1} of AuNPs. Subsequently, we proceeded with the PET imaging study. The representative PET image and the region of interest (ROI) analysis reported in Figure 3 show that the [^{18}F]AuNPs displayed a broad biodistribution profile and collected mainly in the liver, lungs, heart, kidneys, and bladder. This was expected because of the small size of the nanoparticles (∼3 nm) and their ethylene glycol coating that prolongs their circulation halftime. However, there are certain aspects that make these [^{18}F]AuNPs unique. More specifically, the ROI analysis confirms that the highest uptake was recorded in the liver and in the bladder.

Whereas the liver showed a high and instantaneous accumulation of AuNPs presumably because of accumulation via the reticuloendothelial system, the bladder displayed a slower and more gradual accumulation over the first 50 min after intravenous injection. This is unusual for particles of this size, which are normally excreted very quickly through the renal pathway, displaying short blood circulation half-life.[53,63] The high accumulation in the lungs suggests that the nanoparticles have been trapped in the vascular bed of the lungs, which is also unusual for 3 nm AuNPs. Taken together, the biodistribution observations suggest that these 3 nm AuNPs behave in a balanced manner, with renal excretion occurring concomitantly with retention in the liver and lungs. It is possible that a level of aggregation is occurring in vivo, resulting in the unexpected liver and lung retention, as this is typically seen only for AuNPs of >5.5 nm hydrodynamic environment. Whereas a recent report indicates limited brain uptake for small AuNPs (0.07−0.13% ID/g),[64] brain uptake does not appear to be significant in this instance for the

DOI: 10.1021/acsomega.9b02322
ACS Omega 2019, 4, 19106−19115

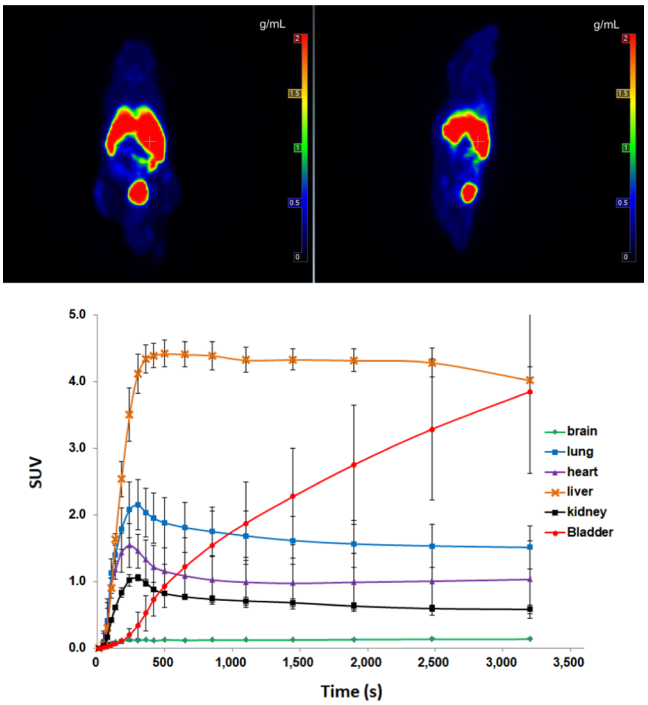

Figure 3. Top: PET image of [^{18}F]AuNPs at 40−60 min after intravenous injection in C57/B6 mouse, coronal image (left) sagittal image (right). Bottom: SUV curves at 1 h postinjection, n = 2.

PEGylated and nitrone-modified construct and is instead similar to reports for slightly larger AuNPs.[38,39] These findings show that the [^{18}F]AuNPs represent a promising template for the development of PET imaging agents, as they have a relatively nonspecific biodistribution and long retention time. These characteristics combined with our ability to control at the molecular level the functionalization of the AuNP's corona make this nanomaterial ideal for the development of PET imaging agents for in vivo targeting of cancer or other disease states.

CONCLUSIONS

In summary, we reported a new methodology for the synthesis of nanomaterial-based PET contrast agents that is based on the use of bioorthogonal nanomaterial templates. We synthesized a new bioorthogonal AuNP template based on small (∼3 nm) amphiphilic AuNPs with interfacial nitrone functionalities. The nitrone−AuNPs were fully characterized using a variety of techniques including ^{1}H NMR spectroscopy, TGA, TEM, and XPS, and the amount of interfacial nitrone moieties was calculated with good precision using independent methods. Furthermore, the amount of interfacial nitrone moieties can be carefully tuned through the ligand exchange reaction and their number determined through the methodology reported here. Changing the amount of interfacial nitrone groups has an impact on the solubility properties of the final nanoparticle, with the possibility of making it water-soluble, amphiphilic, or organic solvent-soluble, depending on the desired application.

For the first time, we then showcased the utility of the I-SPANC reaction and bioorthogonal nanomaterial templates for the preparation of a radiolabeled probe. We prepared ^{18}F-labeled AuNPs by reacting the nitrone groups present on the nanoparticle's surface with a radiolabeled prosthetic group incorporating a strained alkyne. The I-SPANC reaction was quantitative when using the ^{19}F-surrogate and the prosthetic group was covalently bound to the nanocarrier. Most importantly, the final [^{18}F]AuNPs retained their water-solubility despite the lipophilicity of the prosthetic group, thanks to the ability of the nitrone−AuNP template to act as phase-transfer agent. The resulting PET imaging agent was then tested in vivo, which displayed broad biodistribution, and relatively low uptake in background organs of the kidney, lung, and heart.

Importantly, through employing an AuNP nanocarrier, one can overcome the limitations of injecting "free" radiolabeled agents directly, which are often disadvantaged because of nonspecific biodistribution, and limited tunability of their structural and chemical properties. Instead, nitrone−AuNPs represent a versatile tool on which simultaneous and multivalent attachment of radiolabeled prosthetic groups, biomolecules, and drugs can be achieved with molecular level control. This allows for in vivo targeting or labeling of chemical reporters because of the bioorthogonal nature of I-SPANC. Furthermore, although [^{18}F]-labeled AuNPs are reported here, the generality of the [^{18}F]-BCN prosthetic group and its ability to broadly react with azido and nitrone functionalities on other materials or biomolecules opens unprecedented opportunities for the preparation of more diverse PET imaging tools via simple "pour and mix" chemistry.

MATERIALS AND METHODS

The following reagents were used as received. Triethylene glycol monomethylether (MeO−EG$_3$−OH), tetraethylene glycol (HO−EG$_4$−OH), 4-dimethylaminopyridine (DMAP), potassium thioacetate, deuterated acetonitrile (CD_3CN), deuterated chloroform ($CDCl_3$), phosphorous pentoxide (P_2O_5), tetrachloroauric acid trihydrate ($HAuCl_4{\cdot}3H_2O$), sodium borohydride ($NaBH_4$), *p*-toluenesulfonyl chloride (TosCl), *N*-methylhydroxylamine hydrochloride ($CH_3NHOH{\cdot}HCl$), sodium azide (NaN_3), triphenylmethanethiol ($HSCPh_3$), triisopropylsilane (TIPS), *N*,*N*-Diisopropylethylamine (DIPEA), phthalimide potassium, sodium iodide (NaI), hydrazine monohydrate ($H_2N{-}NH_2{\cdot}H_2O$), cesium fluoride (CsF), and *O*-(benzotriazole-1-yl)-*N*,*N*,*N*′,*N*′-tetramethyluronium hexafluorophosphate (HBTU) were purchased from Sigma-Aldrich. All common solvents, triethyleneamine (Et_3N), sodium sulfate anhydrous (Na_2SO_4), dry methanol (CH_3OH), *tert*-butanol (*t*BuOH), hydrochloric acid (HCl), TFA, sodium hydroxide (NaOH), sodium bicarbonate ($NaHCO_3$) and potassium carbonate (K_2CO_3) were purchased from Caledon. Deuterated water (D_2O) was purchased from Cambridge Isotope Laboratories. Ethanol (EtOH) was purchased from Commercial Alcohols. Glacial acetic acid (99.7%) was purchased from BDH. Dialysis membranes (MWCO 6000−8000) were purchased from Spectra/Por.

^{18}F-Fluoride was obtained from the Nordal Cyclotron & PET Radiochemistry Facility at the Lawson Health Research Institute, London, Canada. An automated synthesis unit (TRACERlab, GE Healthcare, Schenectady, NY) was used to prepare and purify [^{18}F] SA-64. A V-10 evaporator (Biotage, Charlotte, NC) was used to remove the solvent after high-performance liquid chromatography (HPLC) purification. A PD-10 desalting column was purchased from GE Healthcare. HPLC analysis and purification was performed on a Waters HPLC system (Milford, MA) using a dual detector system (UV and radiometric), with the mobile phase being CH_3CN

DOI: 10.1021/acsomega.9b02322
ACS Omega 2019, 4, 19106−19115

(solvent A)/H_2O (solvent B) containing 0.1% TFA. The HPLC columns were as follows: Sunfire RP-18 analytical column (Waters): 4.6 × 250 mm, 5 μm, flow rate: 1.5 mL/min; Sunfire RP-18 semipreparative column (Waters): 10 × 250 mm, 5 μm, flow rate: 4 mL/min. The UV detector was set to λ_{max} = 230 nm. C57/B6 mice (male, 10−12 weeks age) were ordered from Charles River (Wilmington, MA) for PET imaging. All animal studies were performed following the Canadian Council on Animal Care guidelines and animal use protocol approved by the animal facility of Western University. Imaging was performed using the Inveon preclinical PET system (Siemens Medical Solutions, Knoxville TN) on age-matched littermate mice using list mode scanning. Acquisition, histograms, and reconstructions were all performed using the Siemens Inveon acquisition and reconstruction software supplied with the scanner.

^{1}H, and ^{13}C and ^{19}F $\{^{1}H\}$ NMR spectra were recorded on either a Varian Inova 400 MHz, Varian Inova 600 MHz, or a Varian Mercury 400 MHz spectrometer and were calibrated against the residual protonated solvents. TEM images were recorded from a TEM Philips CM10. The TEM grids (Formvar carbon film on 400 mesh copper grids) were purchased from Electron Microscopy Sciences and prepared by drop-casting a solution of nanoparticles directly onto the grid surface. Mass spectrometry measurements were carried out using a Micro mass LCT (electrospray time-of-flight) mass spectrometer. TGA measurements were recorded by loading the sample in a 70 μL ceramic crucible and heating from 25 to 750 °C with a rate of 10 °C min^{-1}. The experiments were performed under a nitrogen flow of 70 mL min^{-1} in a Mettler Toledo TGA/SDTA 851 instrument. The XPS analyses were carried out with a Kratos Axis Ultra spectrometer using a monochromatic Al Kα source (15 mA, 14 kV). The instrument work function was calibrated to give a BE of 83.96 eV for the Au $4f_{7/2}$ line for metallic gold and the spectrometer dispersion was adjusted to give a BE of 932.62 eV for the Cu $2p_{3/2}$ line of metallic copper. Specimens were mounted on a double-sided adhesive tape and the Kratos charge neutralizer system was used on all specimens. Survey scan analyses were carried out with an analysis area of 300 × 700 microns and pass energy of 160 eV. High-resolution analyses were carried out with an analysis area of 300 × 700 microns and pass energy of 20 eV. Spectra have been charge-corrected when needed to the main line of the carbon 1s spectrum set to 285.0 eV for aliphatic carbon. Spectra were analyzed using CasaXPS software (version 2.3.14). UV−vis spectra were collected employing a Varian Cary 300 Bio spectrometer in CH_3CN. The FTIR spectra were carried out using KBr pellets on a Bruker VECTOR33 spectrometer.

Synthetic details and additional characterization data of molecules and AuNPs can be found in the Supporting Information.

■ ASSOCIATED CONTENT

Supporting Information

The Supporting Information is available free of charge on the ACS Publications website at DOI: 10.1021/acsomega.9b02322.

Details of synthetic procedures and characterization data of compounds and details of the AuNP raw formula calculation (PDF)

■ AUTHOR INFORMATION

Corresponding Authors

*E-mail: lluyt@uwo.ca (L.G.L.).

*E-mail: mworkent@uwo.ca Phone: +1 519-661-2111 ext. 86319 @WorkentinChem (M.S.W.).

ORCID

Leonard G. Luyt: 0000-0002-0941-4731

Mark S. Workentin: 0000-0001-8517-6483

Present Addresses

‖P.G., School of Chemistry, The University of Bristol, Bristol, UK.

⊥A.N., Département de chimie, Université du Québec à Montreal, Montreal, Québec.

Notes

The authors declare no competing financial interest.

■ ACKNOWLEDGMENTS

We acknowledge financial support from the Natural Sciences and Engineering Research Council of Canada and The University of Western Ontario. P.G. thanks the Government of Canada for a Vanier Scholarship and Research Western.

■ ABBREVIATIONS

AuNPs, gold nanoparticles; FT-IR, Fourier transform infrared (spectroscopy); I-SPAAC, interfacial strain-promoted alkyne−azide cycloaddition; I-SPANC, interfacial strain-promoted alkyne−nitrone cycloaddition; NMR, nuclear magnetic resonance (spectroscopy); TEG−AuNP, triethylene glycol monomethyl ether-modified AuNP; TEM, transmission electron microscopy; TFA, trifluoroacetic acid; TGA, thermogravimetric analysis; XPS, X-ray photoelectron spectroscopy

■ REFERENCES

(1) Phelps, M. E. Positron emission tomography provides molecular imaging of biological processes. *Proc. Natl. Acad. Sci. U.S.A.* **2000**, *97*, 9226−9233.

(2) Massoud, T. F.; Gambhir, S. S. Molecular imaging in living subjects: seeing fundamental biological processes in a new light. *Genes Dev.* **2003**, *17*, 545−580.

(3) Paans, A. Positron emission tomography: the conceptual idea using a multidisciplinary approach. *Methods* **2002**, *27*, 195.

(4) McCarthy, T. J.; Schwarz, S. W.; Welch, M. J. Nuclear medicine and positron emission tomography: an overview. *J. Chem. Educ.* **1994**, *71*, 830−836.

(5) Czernin, J.; Phelps, M. E. Positron emission tomography scanning: Current and future applications. *Annu. Rev. Med.* **2002**, *53*, 89−112.

(6) Fowler, J. S.; Wolf, A. P. Working against time: Rapid radiotracer synthesis and imaging the human brain. *Acc. Chem. Res.* **1997**, *30*, 181−188.

(7) Kettenbach, K.; Schieferstein, H.; Ross, T. L. 18F-labeling using click cycloadditions. *BioMed Res. Int.* **2014**, *2014*, 361329.

(8) Bouvet, V.; Wuest, M.; Wuest, F. Copper-free click chemistry with the short-lived positron emitter fluorine-18. *Org. Biomol. Chem.* **2011**, *9*, 7393−7399.

(9) Campbell-Verduyn, L. S.; Mirfeizi, L.; Schoonen, A. K.; Dierckx, R. A.; Elsinga, P. H.; Feringa, B. L. Strain-promoted copper-free "click" chemistry for 18F radiolabeling of bombesin. *Angew. Chem., Int. Ed. Engl.* **2011**, *50*, 11117−11120.

(10) Arumugam, S.; Chin, J.; Schirrmacher, R.; Popik, V. V.; Kostikov, A. P. [^{18}F]Azadibenzocyclooctyne ([^{18}F]ADIBO): A biocompatible radioactive labeling synthon for peptides using catalyst free [3+2] cycloaddition. *Bioorg. Med. Chem. Lett.* **2011**, *21*, 6987−6991.

DOI: 10.1021/acsomega.9b02322
ACS Omega 2019, 4, 19106−19115

(11) Boudjemeline, M.; McNitt, C. D.; Singleton, T. A.; Popik, V. V.; Kostikov, A. P. [^{18}F]ODIBO: a prosthetic group for bioorthogonal radiolabeling of macromolecules via strain-promoted alkyne−azide cycloaddition. *Org. Biomol. Chem.* **2018**, *16*, 363−366.
(12) Murrell, E.; Kovacs, M. S.; Luyt, L. G. A Compact and Synthetically Accessible Fluorine-18 Labelled Cyclooctyne Prosthetic Group for Labelling of Biomolecules by Copper-Free Click Chemistry. *ChemMedChem* **2018**, *13*, 1625−1628.
(13) Carpenter, R. D.; Hausner, S. H.; Sutcliffe, J. L. Copper-Free Click for PET Rapid 1,3-Dipolar Cycloadditions with a Fluorine-18 Cyclooctyne. *ACS Med. Chem. Lett.* **2011**, *2*, 885−889.
(14) Hausner, S. H.; Carpenter, R. D.; Bauer, N.; Sutcliffe, J. L. Evaluation of an integrin $\alpha_v\beta_6$-specific peptide labeled with [^{18}F] fluorine by copper-free, strain-promoted click chemistry. *Nucl. Med. Biol.* **2013**, *40*, 233−239.
(15) Zhou, Z.; Chitneni, S. K.; Devoogdt, N.; Zalutsky, M. R.; Vaidyanathan, G. Fluorine-18 labeling of an anti-HER2 VHH using a residualizing prosthetic group via a strain-promoted click reaction Chemistry and preliminary evaluation. *Bioorg. Med. Chem.* **2018**, *26*, 1939−1949.
(16) Evans, H. L.; Slade, R. L.; Carroll, L.; Smith, G.; Nguyen, Q.-D.; Iddon, L.; Kamaly, N.; Stöckmann, H.; Leeper, F. J.; Aboagye, E. O.; Spivey, A. C. Copper-free click—a promising tool for pre-targeted PET imaging. *Chem. Commun.* **2012**, *48*, 991−993.
(17) Sachin, K.; Jadhav, V. H.; Kim, E.-M.; Kim, H. L.; Lee, S. B.; Jeong, H.-J.; Lim, S. T.; Sohn, M.-H.; Kim, D. W. F-18 Labeling Protocol of Peptides Based on Chemically Orthogonal Strain-Promoted Cycloaddition under Physiologically Friendly Reaction Conditions. *Bioconjugate Chem.* **2012**, *23*, 1680−1686.
(18) Kim, H. L.; Sachin, K.; Jeong, H. J.; Choi, W.; Lee, H. S.; Kim, D. W. F-18 Labeled RGD Probes Based on Bioorthogonal Strain-Promoted Click Reaction for PET Imaging. *ACS Med. Chem. Lett.* **2015**, *6*, 402−407.
(19) Agard, N. J.; Prescher, J. A.; Bertozzi, C. R. A strain-promoted [3 + 2] azide-alkyne cycloaddition for covalent modification of biomolecules in living systems. *J. Am. Chem. Soc.* **2004**, *126*, 15046−15047.
(20) Ning, X.; Guo, J.; Wolfert, M. A.; Boons, G.-J. Visualizing metabolically labeled glycoconjugates of living cells by copper-free and fast huisgen cycloadditions. *Angew. Chem., Int. Ed. Engl.* **2008**, *47*, 2253−2255.
(21) Dommerholt, J.; Schmidt, S.; Temming, R.; Hendriks, L. J. A.; Rutjes, F. P. J. T.; van Hest, J. C. M.; Lefeber, D. J.; Friedl, P.; van Delft, F. L. Readily accessible bicyclononynes for bioorthogonal labeling and three-dimensional imaging of living cells. *Angew. Chem., Int. Ed. Engl.* **2010**, *49*, 9422−9425.
(22) Zlatopolskiy, B. D.; Kandler, R.; Kobus, D.; Mottaghy, F. M.; Neumaier, B. Beyond azide-alkyne click reaction: easy access to 18F-labelled compounds via nitrile oxide cycloadditions. *Chem. Commun.* **2012**, *48*, 7134−7136.
(23) McKay, C. S.; Moran, J.; Pezacki, J. P. Nitrones as dipoles for rapid strain-promoted 1,3-dipolar cycloadditions with cyclooctynes. *Chem. Commun.* **2010**, *46*, 931−933.
(24) McKay, C. S.; Blake, J. A.; Cheng, J.; Danielson, D. C.; Pezacki, J. P. Strain-promoted cycloadditions of cyclic nitrones with cyclooctynes for labeling human cancer cells. *Chem. Commun.* **2011**, *47*, 10040−10042.
(25) Ning, X.; Temming, R. P.; Dommerholt, J.; Guo, J.; Ania, D. B.; Debets, M. F.; Wolfert, M. A.; Boons, G.-J.; van Delft, F. L. Protein modification by strain-promoted alkyne-nitrone cycloaddition. *Angew. Chem., Int. Ed. Engl.* **2010**, *49*, 3065−3068.
(26) Temming, R. P.; Eggermont, L.; van Eldijk, M. B.; van Hest, J. C. M.; van Delft, F. L. N-Terminal dual protein functionalization by strain-promoted alkyne-nitrone cycloaddition. *Org. Biomol. Chem.* **2013**, *11*, 2772−2779.
(27) Ledin, P. A.; Kolishetti, N.; Boons, G.-J. Multi-Functionalization of Polymers by Strain-Promoted Cycloadditions. *Macromolecules* **2013**, *46*, 7759−7768.
(28) Knight, J. C.; Cornelissen, B. Bioorthogonal chemistry: implications for pretargeted nuclear (PET/SPECT) imaging and therapy. *Am. J. Nucl. Med. Mol. Imaging* **2014**, *4*, 96−113.
(29) Liu, Y.; Welch, M. J. Nanoparticles labeled with positron emitting nuclides: advantages, methods, and applications. *Bioconjugate Chem.* **2012**, *23*, 671−682.
(30) Hahn, M. A.; Singh, A. K.; Sharma, P.; Brown, S. C.; Moudgil, B. M. Nanoparticles as contrast agents for in-vivo bioimaging: current status and future perspectives. *Anal. Bioanal. Chem.* **2011**, *399*, 3−27.
(31) Kim, C. S.; Tonga, G. Y.; Solfiell, D.; Rotello, V. M. Inorganic nanosystems for therapeutic delivery: status and prospects. *Adv. Drug Delivery Rev.* **2013**, *65*, 93−99.
(32) Mieszawska, A. J.; Mulder, W. J. M.; Fayad, Z. A.; Cormode, D. P. Multifunctional gold nanoparticles for diagnosis and therapy of disease. *Mol. Pharm.* **2013**, *10*, 831−847.
(33) Shah, M.; Badwaik, V. D.; Dakshinamurthy, R. Biological applications of gold nanoparticles. *J. Nanosci. Nanotechnol.* **2014**, *14*, 344−362.
(34) Dykman, L.; Khlebtsov, N. Gold nanoparticles in biomedical applications: recent advances and perspectives. *Chem. Soc. Rev.* **2012**, *41*, 2256−2282.
(35) Agarwal, A.; Shao, X.; Rajian, J. R.; Zhang, H.; Chamberland, D. L.; Kotov, N. A.; Wang, X. Dual-mode imaging with radiolabeled gold nanorods. *J. Biomed. Opt.* **2011**, *16*, 051307.
(36) Sun, X.; Huang, X.; Yan, X.; Wang, Y.; Guo, J.; Jacobson, O.; Liu, D.; Szajek, L. P.; Zhu, W.; Niu, G.; Kiesewetter, D. O.; Sun, S.; Chen, X. Chelator-Free Cu-64-Integrated Gold Nanomaterials for Positron Emission Tomography Imaging Guided Photothermal Cancer Therapy. *ACS Nano* **2014**, *8*, 8438−8446.
(37) Lu, W.; Zhang, G.; Zhang, R.; Flores, L. G., II; Huang, Q.; Gelovani, J. G.; Li, C. Tumor site-specific silencing of NF-kappaB p65 by targeted hollow gold nanosphere-mediated photothermal transfection. *Cancer Res.* **2010**, *70*, 3177−3188.
(38) Shao, X.; Agarwal, A.; Rajian, J. R.; Kotov, N. A.; Wang, X. Synthesis and bioevaluation of (1)(2)(5)I-labeled gold nanorods. *Nanotechnology* **2011**, *22*, 135102.
(39) Guerrero, S.; Herance, J. R.; Rojas, S.; Mena, J. F.; Gispert, J. D.; Acosta, G. A.; Albericio, F.; Kogan, M. J. Synthesis and in vivo evaluation of the biodistribution of a 18F-labeled conjugate gold-nanoparticle-peptide with potential biomedical application. *Bioconjugate Chem.* **2012**, *23*, 399−408.
(40) De Jong, W. H.; Hagens, W. I.; Krystek, P.; Burger, M. C.; Sips, A. J. A. M.; Geertsma, R. E. Particle size-dependent organ distribution of gold nanoparticles after intravenous administration. *Biomaterials* **2008**, *29*, 1912−1919.
(41) Del Pino, P.; Yang, F.; Pelaz, B.; Zhang, Q.; Kantner, K.; Hartmann, R.; Martinez de Baroja, N.; Gallego, M.; Moller, M.; Manshian, B. B.; Soenen, S. J.; Riedel, R.; Hampp, N.; Parak, W. J. Basic Physicochemical Properties of Polyethylene Glycol Coated Gold Nanoparticles that Determine Their Interaction with Cells. *Angew. Chem., Int. Ed.* **2016**, *55*, 5483−5487.
(42) Zhao, Y.; Sultan, D.; Detering, L.; Cho, S.; Sun, G.; Pierce, R.; Wooley, K. L.; Liu, Y. Copper-64-alloyed gold nanoparticles for cancer imaging: improved radiolabel stability and diagnostic accuracy. *Angew. Chem., Int. Ed. Engl.* **2014**, *53*, 156−159.
(43) Wang, Y.; Liu, Y.; Luehmann, H.; Xia, X.; Wan, D.; Cutler, C.; Xia, Y. Radioluminescent gold nanocages with controlled radioactivity for real-time in vivo imaging. *Nano Lett.* **2013**, *13*, 581−585.
(44) Xie, H.; Wang, Z. J.; Bao, A.; Goins, B.; Phillips, W. T. In vivo PET imaging and biodistribution of radiolabeled gold nanoshells in rats with tumor xenografts. *Int. J. Pharm.* **2010**, *395*, 324−330.
(45) Zhang, G.; Yang, Z.; Lu, W.; Zhang, R.; Huang, Q.; Tian, M.; Li, L.; Liang, D.; Li, C. Influence of anchoring ligands and particle size on the colloidal stability and in vivo biodistribution of polyethylene glycol-coated gold nanoparticles in tumor-xenografted mice. *Biomaterials* **2009**, *30*, 1928−1936.
(46) Gobbo, P.; Luo, W.; Cho, S. J.; Wang, X.; Biesinger, M. C.; Hudson, R. H. E.; Workentin, M. S. Small gold nanoparticles for

DOI: 10.1021/acsomega.9b02322
ACS Omega 2019, 4, 19106−19115

interfacial Staudinger-Bertozzi ligation. *Org. Biomol. Chem.* **2015**, *13*, 4605−4612.
(47) Gobbo, P.; Novoa, S.; Biesinger, M. C.; Workentin, M. S. Interfacial strain-promoted alkyne-azide cycloaddition (I-SPAAC) for the synthesis of nanomaterial hybrids. *Chem. Commun.* **2013**, *49*, 3982−3984.
(48) Gobbo, P.; Mossman, Z.; Nazemi, A.; Niaux, A.; Biesinger, M. C.; Gillies, E. R.; Workentin, M. S. Versatile strained alkyne modified water-soluble AuNPs for interfacial strain promoted azide-alkyne cycloaddition (I-SPAAC). *J. Mat. Chem. B* **2014**, *2*, 1764−1769.
(49) Wang, X.; Gobbo, P.; Suchy, M.; Workentin, M. S.; Hudson, R. H. E. Peptide-decorated gold nanoparticles via strain-promoted azide-alkyne cycloaddition and post assembly deprotection. *RSC Adv.* **2014**, *4*, 43087−43091.
(50) Luo, W.; Gobbo, P.; Gunawardene, P. N.; Workentin, M. S. Fluorogenic Gold Nanoparticle (AuNP) Substrate: A Model for the Controlled Release of Molecules from AuNP Nanocarriers via Interfacial Staudinger−Bertozzi Ligation. *Langmuir* **2017**, *33*, 1908−1913.
(51) Luo, W.; Gobbo, P.; McNitt, C. D.; Sutton, D. A.; Popik, V. V.; Workentin, M. S. "Shine & Click" Photo-Induced Interfacial Unmasking of Strained Alkynes on Small Water-Soluble Gold Nanoparticles. *Chem.—Eur. J.* **2017**, *23*, 1052−1059.
(52) Luo, W.; Luo, J.; Popik, V. V.; Workentin, M. S. Dual-Bioorthogonal Molecular Tool: "Click-to-Release" and "Double-Click" Reactivity on Small Molecules and Material Surfaces. *Bioconjugate Chem.* **2019**, *30*, 1140−1149.
(53) Alkilany, A. M.; Murphy, C. J. Toxicity and cellular uptake of gold nanoparticles: what we have learned so far? *J. Nanopart. Res.* **2010**, *12*, 2313−2333.
(54) Weissman, M. R.; Winger, K. T.; Ghiassian, S.; Gobbo, P.; Workentin, M. S. Insights on the Application of the Retro-Michael Addition on Maleimide-Functionalized Gold Nanoparticles in Biology and Nanomedicine. *Bioconjugate Chem.* **2016**, *27*, 586−593.
(55) Gobbo, P.; Workentin, M. S. Improved methodology for the preparation of water-soluble maleimide-functionalized small gold nanoparticles. *Langmuir* **2012**, *28*, 12357−12363.
(56) Lu, J.; Shi, M.; Shoichet, M. S. Click Chemistry Functionalized Polymeric Nanoparticles Target Corneal Epithelial Cells through RGD-Cell Surface Receptors. *Bioconjugate Chem.* **2009**, *20*, 87−94.
(57) Sun, X.-L.; Stabler, C. L.; Cazalis, C. S.; Chaikof, E. L. Carbohydrate and protein immobilization onto solid surfaces by sequential Diels-Alder and azide-alkyne cycloadditions. *Bioconjugate Chem.* **2006**, *17*, 52−57.
(58) Taylor, A.; Wilson, K. M.; Murray, P.; Fernig, D. G.; Lévy, R. Long-term tracking of cells using inorganic nanoparticles as contrast agents: are we there yet? *Chem. Soc. Rev.* **2012**, *41*, 2707−2717.
(59) Gobbo, P.; Biesinger, M. C.; Workentin, M. S. Facile synthesis of gold nanoparticle (AuNP)-carbon nanotube (CNT) hybrids through an interfacial Michael addition reaction. *Chem. Commun.* **2013**, *49*, 2831−2833.
(60) Castner, D. G.; Hinds, K.; Grainger, D. W. X-ray photoelectron spectroscopy sulfur 2p study of organic thiol and disulfide binding interactions with gold surfaces. *Langmuir* **1996**, *12*, 5083−5086.
(61) Milne, M.; Gobbo, P.; McVicar, N.; Bartha, R.; Workentin, M. S.; Hudson, R. H. E. Water-soluble gold nanoparticles (AuNP) functionalized with a gadolinium(III) chelate via Michael addition for use as a MRI contrast agent. *J. Mat. Chem. B* **2013**, *1*, 5628−5635.
(62) Jewett, J. C.; Bertozzi, C. R. Synthesis of a Fluorogenic Cyclooctyne Activated by Cu-Free Click Chemistry. *Org. Lett.* **2011**, *13*, 5937−5939.
(63) Hoshyar, N.; Gray, S.; Han, H.; Bao, G. The effect of nanoparticle size on in vivo pharmacokinetics and cellular interaction. *Nanomedicine* **2016**, *11*, 673−692.
(64) Zhu, J.; Chin, J.; Wängler, C.; Wängler, B.; Lennox, R. B.; Schirrmacher, R. Rapid (18)F-labeling and loading of PEGylated gold nanoparticles for in vivo applications. *Bioconjugate Chem.* **2014**, *25*, 1143−1150.

DOI: 10.1021/acsomega.9b02322
ACS Omega 2019, 4, 19106−19115